V. Muscarello, A. Zanoni, G. Quaranta
Impact of Design and Operational Parameters on Helicopter Vertical Bounce
Journal of the American Helicopter Society, Vol. 68, N. 3, 2023, p. 32009-32022
doi:10.4050/JAHS.68.032009

Impact of Design and Operational Parameters on Helicopter Vertical Bounce

Vincenzo Muscarello*

Senior Lecturer,

Aerospace Engineering and Aviation, RMIT University,

3082 Melbourne, Victoria, Australia

Andrea Zanoni

Assistant Professor,

Dept. of Aerospace Science and Technology, Politecnico di Milano,

20156 Milan, Italy

Giuseppe Quaranta

Full Professor,

Dept. of Aerospace Science and Technology, Politecnico di Milano,

20156 Milan, Italy

Abstract

Vertical bounce is a rotorcraft aeroelastic instability triggered by the feedback interaction between two significantly damped vibration modes: the rotor collective flap mode and the biodynamic vertical oscillation of the pilot's left arm holding the collective lever in the cockpit. The instability can endanger the safety of flight and in some cases led to catastrophic events.

This work develops simple yet complete models that allow us to better understand the dependency of the phenomenon on parameters like the flight condition, the characteristics of the aircraft, and the properties of the pilot's biodynamic feedthrough. The stability analyses presented demonstrate

*Corresponding author (vincenzo.muscarello@rmit.edu.au).

that the landing gear dynamics may amplify the vertical oscillations driven by the pilot's biodynamic response when considering on-ground conditions, reducing the stability margins of the pilot-vehicle system. The detailed sensitivity analysis allows inferring indications to develop future rotorcraft that could be less prone to this adverse rotorcraft-pilot coupling phenomenon.

Nomenclature

C_ℓ	collective lever rotational damping, N·m/rad/s
C_T	collective lever equivalent damping due to the force trim mechanism, N·m/rad/s
c	landing gear viscous coefficient, N·s/m
c_p	equivalent pilot biomechanical viscous coefficient, N·s/m
G_0	gear ratio between collective lever position and collective pitch rotation
G_m	gain margin, dB
g	gravity acceleration, m/s^2
$H_{\ddot{z}\vartheta_0}$	helicopter transfer function
H_{BDFT}	pilot biodynamic feedthrough
H_{LTF}	loop transfer function
H_{NMA}	pilot neuromuscular admittance
I_β	blade inertia moment about the flap hinge, Kg·m^2
J_ℓ	collective lever equivalent inertia, Kg·m^2
K_ℓ	collective lever rotational stiffness, N·m/rad
K_T	collective lever equivalent stiffness due to the force trim mechanism, N·m/rad
k	landing gear stiffness, N/m
k_p	equivalent pilot biomechanical stiffness, N/m
ℓ	collective lever length, m
M	moment acting on the collective control lever, N·m
m	helicopter mass, Kg
m_ℓ	collective lever mass, Kg

m_p	equivalent pilot biomechanical mass, Kg
N_b	number of blades
P_m	phase margin, deg
R	rotor radius, m
S_β	blade static moment about the flap hinge, Kg·m
S_ℓ	collective lever static moment about pivot point, Kg·m
x_{CM}	collective lever center of mass offset, m
z	helicopter vertical displacement, m
β_0	collective flap angle, deg
γ	Lock's number
δ_0	collective lever position, deg
δ_3	pitch-flap coupling, deg
ϑ_0	collective pitch, deg
ν_β	dimensionless flap frequency, /rev
ξ_{LG}	landing gear heave mode damping ratio, %
ξ_p	pilot biomechanical damping ratio, %
Ω	rotor speed, rpm
ω_{LG}	landing gear heave mode natural frequency, Hz
ω_p	pilot biomechanical natural frequency, Hz
$\dot{(\cdot)} = \frac{d}{dt}$	time derivative
$\hat{(\cdot)}$	variable evaluated with the control device dynamics
$(\cdot)_E$	variable evaluated at the equilibrium condition

Introduction

Rotorcraft-Pilot Couplings (RPCs), namely, adverse interactions of the pilot with rotorcraft aeromechanics, are potentially dangerous phenomena. During RPCs, the pilot, as a consequence of misleading or incorrectly interpreted cues, operates the control inceptors in a manner that produces inadvertent or unin-

tentional commands. These commands, in turn, can produce a behavior of the vehicle that causes further misleading cues, and induce additional adverse input, potentially resulting in unstable events (Ref. 1).

A well-known class of RPC phenomena is caused by the pilot's erroneous perception of the vehicle dynamics that can lead to pilot-induced oscillations (PIOs), where the main cause is a voluntary, out-of-phase, control input introduced by the pilot (Ref. 2). However, a second kind of feedback loop is also possible, caused by the vibrations that are injected in the cockpit by rotor loads and transmitted through the pilot's body into the inceptors. In this case, it is the involuntary movement of the pilot's limb that injects motions into the inceptors that is at the base of this phenomenon, usually indicated in the literature as pilot-assisted oscillations (PAOs), to highlight the transmission role of the pilot. This feedback loop, when unstable, generates divergent oscillations that usually fall in the frequency range between 2–8 Hz (Ref. 3), a range where several rotorcraft structural dynamics modes are located. In many cases, PAOs are influenced by the voluntary pilot behavior too, as is the case when carrying out tasks that require precision, and/or intensive workload. The central nervous system (CNS) activates the muscles to not only provide motion control to the hands and limbs but also to alter their impedance, by modulating the contraction of agonist and antagonist muscles. In fact, human body muscles are systems that can only pull by contraction, so they work in joint pairs: one muscle, the agonist, contracts while the other, the antagonist, relaxes or lengthens. Generally, when greater precision is required, the CNS activates the involved motor units to increase the equivalent mechanical impedance, an effect that is ordinarily felt as a diffused tension, or stiffening of the affected body parts (Ref. 4). So, detailed knowledge and understanding of the pilot's biodynamics is important to understand and prevent PAOs.

Several occurrences of PAO instabilities experienced by US Navy rotorcraft are reported by Walden in Ref. 5. In Europe, Hamel, and Ockier (Refs. 6, 7) reported some critical RPC problems encountered with the German Aerospace Center's (DLR) ATTHeS (Advanced Technologies Testing Helicopter System) system, a modified BO105 helicopter equipped with a full authority non-redundant fly-by-wire (FBW) control system for the main rotor and fly-by-light system for the tail rotor. In July 2016, a biomechanical feedback has been recorded on the Bell 525 Relentless, a modern FBW medium-weight helicopter, while flight testing a series of one-engine-inoperative conditions at increasing airspeeds (Ref. 8). The test induced a scissors-mode vibration in the main rotor, which resulted in involuntary collective control

input. The unintended biomechanical feedback loop exacerbated the vibration, until the rotor contacted the tail boom, resulting in a fatal accident. PAO occurrences on the longitudinal and lateral axes are often less critical since changes in cyclic pitch control do not cause immediate horizontal force imbalance, but rather pitch/roll moments, which are usually filtered by the low-pass behavior of the main rotor in most conventional rotorcraft, especially articulated ones. However, the lateral axis tends to be also critical for PAO especially when a stability augmentation system (SAS) or a flight control system (FCS) is included in the pilot–vehicle system (PVS, Refs. 9, 10). Prediction and simulator verification of roll/lateral adverse aeroservoelastic RPCs are discussed in Ref. 11 for a soft-in-plane hingeless helicopter, where the lightly damped regressive lead–lag mode strongly interacted with the roll mode at a frequency within the biodynamic band of the pilots.

Tiltrotors too have suffered from several PAO events. Aeroservoelastic pilot-in-the-loop coupling phenomena for the V-22 Osprey are described by Parham et al. in Ref. 12. A more complete analysis of all PAO phenomena that can happen on a tiltrotor, without considering the interaction with the FCS, can be found in Ref. 13. The inclusion of the FCS, together with the pilot's biodynamics, in tiltrotor aeroservoelastic stability in the airplane flight regime is discussed in Ref. 14.

The present work investigates the effect of the flexible airframe, specifically related to the landing gear, on the vertical bounce phenomenon. It is speculated that the landing gear dynamics may amplify the vertical oscillations driven by the pilot's biodynamic response through the mechanism already encountered in Ref. 15. It must be remarked that, during a vertical bounce phenomenon, a change in collective pitch essentially results in a very quick change in thrust, producing a vertical acceleration. If the pilot's biomechanics, at least in part, transforms this acceleration into a rotation of the collective inceptor, inducing further changes in rotor blade collective pitch, a feedback loop appears that may lead to unstable events. In ground conditions, the heave mode of the landing gear may produce an additional acceleration, further reducing the stability margins of the PVS. To investigate the vertical bounce phenomenon, pilot/control device biomechanical models must be introduced in the feedback loop with the helicopter dynamics. In this work, detailed yet simple physics-based models of pilots are exploited, to characterize the pilot's unintentional contribution to the collective lever related to the cockpit vertical acceleration, namely the pilot's biodynamics feedthrough (BDFT). The layout of the cockpit and the collective lever is considered

too, including the inertial parameters of the inceptor and the balancing and trim retaining systems characteristics that are among the most important factors that influence the insurgence of dangerous PAO. An extended sensitivity analysis is carried out, considering both the main parameters related to the helicopter and the pilot's BDFT, to provide guidelines for design and means of prevention to be implemented for the next generations of helicopters.

The paper proceeds as follows: the first section is dedicated to the description of the PVS, combining a simplified model of the helicopter heave and rotor coning dynamics, with a pilot-control device structural model including the collective lever mechanical properties. Then, closed-loop stability analyses are carried out and results are discussed, highlighting the role of the landing gear in vertical bounce proneness. The sensitivity analysis, considering the effect of helicopter, pilot anthropometric, and collective control device parameters can be found in the last section. Finally, design guidelines and possible means of prevention to avoid vertical bounce phenomena are discussed.

The Pilot-Control Device-Vehicle System

Helicopter dynamics analytical model

The simplified helicopter model used for preliminary vertical bounce investigation consists of the airframe vertical motion, z, and the main rotor collective flap angle, or rotor coning, β_0. The model, originally proposed in Ref. 15, is modified with a vertical spring-dashpot element between the airframe and the ground, representing the landing gear, as shown in Fig. 1.

The helicopter model is simplified, since it neglects the details of the rotor hub geometry and kinematics, the drive train dynamics, and many details of basic rotor aerodynamics like inflow, twist, tip loss, etc., that may be significant in performance analysis but are considered inessential for the model necessary to infer general design guidelines. The interaction of the main rotor wake with the fuselage and tail surfaces of the helicopter in hover may be significant. However, the relevant phenomena are either static, influencing the value of rotor thrust and pitch moment to trim the aircraft, or concentrated at frequencies that are equal to N_b times the rotor angular speed, where N_b is the number of blades (Ref. 16). Since the frequency range of interest in this study is around 1/rev, these interactions between the main rotor

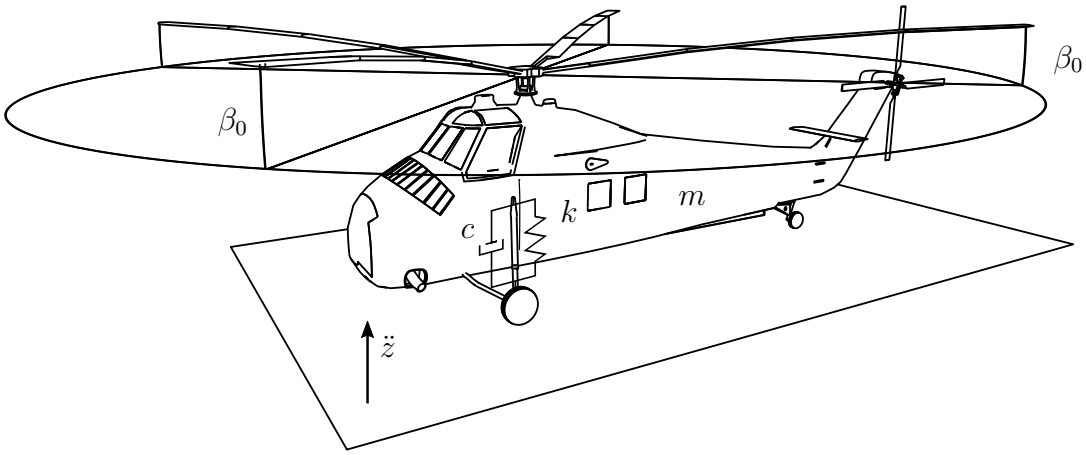

Fig. 1 Sketch of the minimal analytical model of the helicopter associated with pure heave (z) and collective coning (β_0) motion.

wake and the fuselage/empennage have been considered negligible. The validity of these assumptions was verified in Ref. 15, using numerical models obtained from comprehensive rotorcraft analysis. The simplified model is appropriate to capture the vertical bounce phenomenon in hover while it may not be suitable in forward flight, where the vertical motion is strongly coupled with both the longitudinal and lateral-directional dynamics of the helicopter (Ref. 15). When considering take-off or landing maneuvers on horizontal flat ground, the main rotor trim is essentially characterized by axial flow conditions, and the proposed analytical model correctly represents the analyzed configuration. The linearized equations of motion are the following:

$$\begin{bmatrix} m & N_b S_\beta \\ N_b S_\beta & N_b I_\beta \end{bmatrix} \begin{Bmatrix} \ddot{z} \\ \ddot{\beta}_0 \end{Bmatrix} + \begin{bmatrix} \frac{N_b \gamma \Omega I_\beta}{4R^2} + c & \frac{N_b \gamma \Omega I_\beta}{6R} \\ \frac{N_b \gamma \Omega I_\beta}{6R} & \frac{N_b \gamma \Omega I_\beta}{8} \end{bmatrix} \begin{Bmatrix} \dot{z} \\ \dot{\beta}_0 \end{Bmatrix} + \begin{bmatrix} k & 0 \\ 0 & N_b \Omega^2 I_\beta \hat{\nu}_\beta^2 \end{bmatrix} \begin{Bmatrix} z \\ \beta_0 \end{Bmatrix} = N_b \gamma \Omega^2 I_\beta \begin{Bmatrix} \frac{1}{6R} \\ \frac{1}{8} \end{Bmatrix} \vartheta_0 \tag{1}$$

where the viscous coefficient, $c = 2 \cdot m \cdot \xi_{LG} \cdot \omega_{LG}$, and the stiffness term, $k = m \cdot \omega_{LG}^2$, of the landing gear have been added to the first of Eqs. 1, which describes the vertical displacement of the helicopter. With this simplified approach, the landing gear is considered in uninterrupted contact with the ground, and the whole undercarriage structure (including the tires) is condensed into a single spring-damper element,

connecting the helicopter to the ground. The second of Eqs. 1 describes the rotor coning dynamics. The variables z, β_0, and ϑ_0 are linear variations with respect to a reference trim condition. In the following, the simplified helicopter model is essentially seen as a Single Input/Single Output (SISO) system in the Laplace domain, relating the collective pitch input and the helicopter vertical acceleration output, namely:

$$\ddot{z} = H_{\ddot{z}\vartheta_0}(s) \cdot \vartheta_0. \tag{2}$$

The advantage of this model is that it requires few parameters and can therefore be used to run fast parametric analyses, since it is fully expressed in analytical form.

The characteristics of two helicopters with 5-bladed main rotors and articulated hubs have been considered: a medium-heavy lift (MH, 12 tons) and a medium-light lift (ML, 4.1 tons). The first category has been selected since it is more prone to the vertical bounce phenomenon (Ref. 15). The main reason is due to the large rotor radius that requires low rotor speeds. For an articulated rotor, this implies that the rotor collective flap mode typically lies in the lowest frequency range, between 3 – 4 Hz, overlapping the pilot's biomechanical modes bandwidth. The second one is chosen to provide a comparative measure of the influence of vehicle characteristics on the investigated RPC, considering an aircraft that is less prone to PAO. Table 1 lists the nominal characteristics of the helicopter models investigated in the present work. The contribution of the pitch-flap coupling (δ_3 positive pitch-up, flap down) was added to the dimensionless flap frequency, namely $\hat{\nu}_\beta^2 = \nu_\beta^2 + \frac{\gamma}{8}\tan\delta_3$, in Eq. 1. The landing gear stiffness and viscous coefficient have been selected to obtain a helicopter heave motion with a damping ratio of $6\,\%$, for both vehicles, and a natural frequency of $1.3\,\mathrm{Hz}$ for the medium-heavy helicopter, and $2.0\,\mathrm{Hz}$ for the medium-light one, that are representative of their respective classes. When coupled with the rotor coning dynamics, the simplified helicopter model on the ground shows 2 complex (and conjugate) roots. The heave mode frequency does not change significantly, while the corresponding damping ratio increases due to rotor aerodynamics (MH: $13.2\,\%$, ML: $11.4\,\%$). The rotor coning frequency for the MH helicopter is found at $3.5\,\mathrm{Hz}$ and it is characterized by a large damping ratio, equal to $53.6\,\%$. The ML helicopter shows a higher coning frequency at $5.8\,\mathrm{Hz}$, with a damping ratio of $42.7\,\%$. Indeed, neglecting the pilot's biodynamic feedthrough, the two helicopter dynamics are well damped, leading to asymptotically stable systems.

Table 1. Helicopter models parameters.

Parameter	Symbol	Value (MH)	Value (ML)	Units
Total mass	m	12 000	4100	kg
Landing gear damping ratio	ξ_{LG}	6.0	6.0	%
Landing gear natural frequency	ω_{LG}	1.3	2.0	Hz
Number of blades	N_b	5	5	–
Rotor radius	R	9.5	6.0	m
Rotor speed	Ω	205	330	rpm
Lock number	γ	10.7	8.3	–
Flap static moment	S_β	650	120	kg m
Flap inertia moment	I_β	3800	480	kg m^2
Flap frequency	ν_β	1.04	1.04	–
Pitch-flap coupling	δ_3	15.0	15.0	deg

Pilot-control device dynamics

PAO phenomena are generally investigated through the pilot-control device dynamics in feedback loop with the aircraft model. Detailed physics-based pilot models can be developed using first-principles approaches, like multibody modeling (see Refs. 17, 18). Those models are generally nonlinear, require extensive and careful validation, and are characterized by a large number of degrees of freedom. Indeed, the pilot impedance at the control inceptors, which is a function of the pilot's muscular activation, depends on many factors including pilot's biometrics, body posture, mental state and workload, the flight task that is required to perform, etc. (see Ref. 4). Additionally, the control device dynamics must be taken into account, including the contact forces applied by the pilot to reach the required deflections of the inceptors while resisting to inertia, viscous, gravity, and elastic restoring forces.

A different, and in some aspects easier, approach is based on the description of the pilot response through the employment of linear, frequency domain TFs, using data from cockpit mock-up excitation (e.g., Allen et al. – Ref. 19, Jex and Magdaleno – Ref. 20, and Höhne – Ref. 21), flight simulator tests (e.g.,

Mayo – Ref. 22 and Masarati et al. – Ref. 23), or in-flight measurements (e.g., Parham et al. – Ref. 12). Using this approach, it is common to consider separate independent TFs to model the voluntary and involuntary parts of the pilot control action, although, in principle, the pilot model should be represented as a unique dynamic system. However, it is the involuntary part of the pilot response that generates the coupling in the frequency band of interest for PAO events.

In this work, a simpler yet complete analytic model is proposed to model the pilot's involuntary action. The collective lever pitch input δ_0 introduced by the pilot's unintentional action is split in two terms: one, denominated biodynamic feedthrough (BDFT), which is related to the pilot's body and limbs oscillations due to vertical acceleration $\ddot{z}$, when the inceptor is otherwise unloaded, and a second one associated with the torque M_c applied to the inceptor when no vibration affects the cockpit, denominated neuromuscular admittance (NMA). When the two contributions are expressed through a linearized model with respect to a reference condition, it is possible to write their effect in the Laplace domain as

$$\delta_0 = H_{BDFT}(s) \cdot \ddot{z} + H_{NMA}(s) \cdot M_c. \tag{3}$$

The two transfer functions are obtained from the simplified pilot-control device mechanical model depicted in figure 2. The pilot's biomechanics are described by an equivalent mass m_p, viscous coefficient

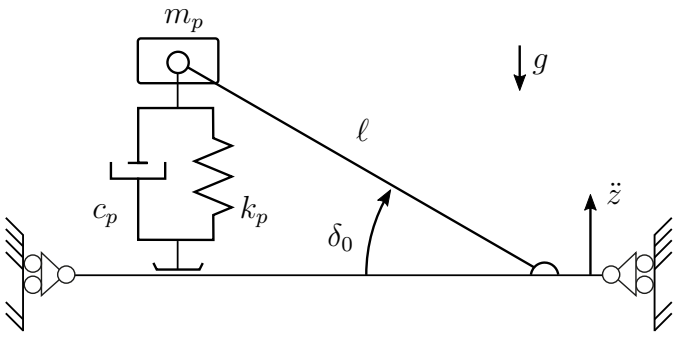

Fig. 2 Equivalent pilot-control device model.

c_p, and stiffness k_p, representing the dominant generalized modal degree of freedom of pilots in the vertical direction. The corresponding frequency and damping ratio are respectively $\omega_p = \sqrt{k_p/m_p}$ and $\xi_p = c_p/\left(2\sqrt{m_p \cdot k_p}\right)$. The model is a generalization of the structural model equivalent to Mayo's functions that describes the involuntary action of the pilot, with the inclusion of a simplified collective lever

device.

The pilot's BDFT and NMA are obtained from the equations of motion of the pilot-control device model shown in Fig. 2, linearized about a reference collective lever condition δ_{0_E}, namely:

$$H_{BDFT}(s) = -\frac{\cos\delta_{0_E}}{\ell}\cdot\frac{1}{s^2 + 2\xi_{p_E}\omega_{p_E}s + \omega_{p_E}^2}, \tag{4a}$$

$$H_{NMA}(s) = -\frac{1}{m_p\ell^2}\cdot\frac{1}{s^2 + 2\xi_{p_E}\omega_{p_E}s + \omega_{p_E}^2}, \tag{4b}$$

with $\omega_{p_E} = \omega_p \cdot \cos\delta_{0_E}$ and $\xi_{p_E} = \xi_p \cdot \cos\delta_{0_E}$. The pilot-control device mechanical model shows how both the pilot's natural frequency and the damping ratio decrease for higher reference collective lever angles. This trend was also observed by Masarati et al. in Ref. 23, who experimentally identified the pilot's BDFT for different reference collective lever positions. It is important to highlight that the pilot's BDFT obtained in Eq. 4a requires only the knowledge of the pilot biomechanical natural frequency and damping ratio. The modal mass, instead, is needed only to define the pilot's NMA.

The TFs of Eq. 4 neglect the mass/inertia properties of the collective lever and could be representative of a balanced lever, whose center of mass is located at the pivot point, with negligible inertia compared to the contribution of the pilot's modal mass, i.e. $J_\ell << m_p\ell^2$. However, the model proposed in Eq. 3 may include the control inceptor dynamics as well if the mechanical properties are known, and if the corresponding generalized moments can be linearized about a reference condition. Eq. 3, in fact, from a design standpoint, can be very useful to analyze how the dynamics of the control device directly affect the pilot's BDFT and NMA, and, subsequently, the overall dynamics of the pilot-vehicle system.

The collective lever dynamics can be added using the single degree of freedom mechanical subsystem sketched in Fig. 3. Its dynamics are described by the equation of motion of a rigid body connected to the floor of the helicopter through a revolute hinge, with the axis considered aligned with the pitch axis of the vehicle. The model is characterized by an equivalent inertia J_ℓ*, mass m_ℓ, and center of mass located at a distance x_{CM} from the revolute hinge. A linear visco-elastic rotational element is included with viscous

*The equivalent inertia J_ℓ is referred to the revolute hinge point. It also includes the transport contribution due to the center of mass offset if the collective lever is not perfectly balanced. In general, it should be determined as the reduced moment of inertia due to the whole collective lever control chain, including all the additional leverages involved in the collective lever motion.

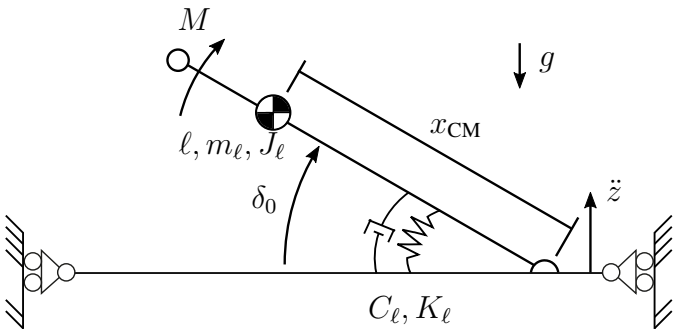

Fig. 3 Mechanical subsystem model of the collective control device.

coefficient C_ℓ and stiffness K_ℓ. The first contribution represents a viscous resistance to the collective lever motion, which could be a rough approximation of the dynamic friction usually introduced to restrain the control device motion. The elastic term is representative of a balancing spring, typically used when the center of mass of the control inceptor does not lie on the hinge axis, to maintain a specific collective lever rest position. The vertical acceleration of the floor $\ddot{z}$ acts as excitation, together with the torque M applied to the lever. The control device equation of motion, linearized about a reference condition, results:

$$J_\ell \ddot{\delta}_0 + C_\ell \dot{\delta}_0 + \left(K_\ell - S_\ell g \sin \delta_{0_E}\right) \delta_0 = -S_\ell \cos \delta_{0_E} \ddot{z} + M, \tag{5}$$

with $S_\ell = m_\ell \cdot x_{\text{CM}}$ and $M = M_c + M_e$, where M_c represents the contribution due to the pilot and M_e any additional moment acting on the device. Eq. 5 can be easily translated in the Laplace domain and combined with Eq. 3 to retrieve the updated pilot's BDFT and NMA, namely:

$$\hat{H}_{BDFT}(s) = -\frac{\cos \delta_{0_E}}{\ell} \frac{1 + S_\ell / (m_p \ell)}{1 + J_\ell / (m_p \ell^2)} \cdot \frac{1}{s^2 + 2\hat{\xi}_{p_E} \hat{\omega}_{p_E} s + \hat{\omega}_{p_E}^2}, \tag{6a}$$

$$\hat{H}_{NMA}(s) = -\frac{1}{m_p \ell^2} \frac{1}{1 + J_\ell / (m_p \ell^2)} \cdot \frac{1}{s^2 + 2\hat{\xi}_{p_E} \hat{\omega}_{p_E} s + \hat{\omega}_{p_E}^2}, \tag{6b}$$

where $\hat{\xi}_{p_E}$ and $\hat{\omega}_{p_E}$ are respectively the damping ratio and the natural frequency of the pilot-control device model, including the control inceptor dynamics

$$\hat{\omega}_{p_E}^2 = \frac{\omega_{p_E}^2 + \left(K_\ell - S_\ell g \sin \delta_{0_E}\right) / (m_p \ell^2)}{1 + J_\ell / (m_p \ell^2)}, \qquad 2\hat{\xi}_{p_E} \hat{\omega}_{p_E} = \frac{2\xi_{p_E} \omega_{p_E} + C_\ell / (m_p \ell^2)}{1 + J_\ell / (m_p \ell^2)}, \tag{7}$$

while the static gain of the pilot's BDFT and NMA become:

$$\hat{H}_{BDFT}(0) = -\frac{\cos\delta_{0_E}}{\ell}\frac{1 + S_\ell/(m_p\ell)}{\omega_{p_E}^2 + (K_\ell - S_\ell g\sin\delta_{0_E})/(m_p\ell^2)}, \tag{8a}$$

$$\hat{H}_{NMA}(0) = -\frac{1}{m_p\ell^2}\frac{1}{\omega_{p_E}^2 + (K_\ell - S_\ell g\sin\delta_{0_E})/(m_p\ell^2)}. \tag{8b}$$

As expected, the elastic term K_ℓ increases the natural frequency of the pilot-control device, while the damping ratio and the static gains are reduced. The introduction of a viscous contribution, C_ℓ, naturally increases the damping ratio. The inertia, J_ℓ, reduces both the natural frequency and the damping ratio. For positive values of the static moment S_ℓ, i.e. when the center of mass of the collective lever is ahead of the rotational axis, the natural frequency decreases, while the damping ratio and the static gain of the pilot's NMA increase. The opposite trend would be obtained if, hypothetically, the center of mass would be located behind the rotational axis. The static gain of the pilot's BDFT depends on S_ℓ both on the numerator and the denominator. Typically, for conventional collective levers, the contribution at the numerator is dominant. So, positive values of the static moment increase the pilot's BDFT static gain. Conversely, a reduction of the pilot's BDFT static gain is observed when S_ℓ decreases.

The reference pilot's biomechanical parameters used in the present work are reported in Table 2, together with the characteristics of a realistic collective lever. The pilot's natural frequency and damping ratio are the same identified by Mayo in Ref. 22, referred to as the ectomorphic pilot with lean and tall build anthropometric characteristics. The pilot's modal mass has been roughly estimated to obtain a force gradient, considering a static reference condition, of about $10\,\mathrm{N/deg}$. Unfortunately, no experimental data is available in the literature related to the measure of the pilot's modal mass, nor for the identification of the pilot's NMA on a collective lever. An experimental work to measure the relationship between the pilot's BDFT and NMA was proposed by Venrooij et al. in Ref. 24, considering different subjects and three control tasks of increasing complexity. The tests were performed on a full-motion flight simulator of a fixed-wing aircraft, thus without a collective lever control inceptor. The identification of the pilot's BDFT and NMA on a collective lever have been presented by Zanlucchi et al. in Ref. 25, using a multibody model of the pilot's left arm. The modal mass, extracted from the pilot's NMA (see Table 1 of Ref. 25), is about $2\,\mathrm{kg}$, i.e. half the value proposed in Table 2. It must be remarked that the multibody model in Ref. 25 only considered the pilot's left arm and not the whole pilot's body. Consequently, it is expected

Table 2. Pilot-control device characteristics.

Characteristic	Symbol	Value	Unit
Pilot's equivalent mass	m_p	4.0	kg
Pilot's damping ratio	ξ_p	32	%
Pilot's natural frequency	ω_p	3.4	Hz
Collective lever length	ℓ	0.350	m
Collective lever min. deflection	$\delta_{0_{min}}$	15.0	deg
Collective lever max. deflection	$\delta_{0_{max}}$	45.0	deg
Collective lever mass	m_ℓ	$2 \cdot 1.50$	kg
Collective lever equivalent inertia	J_ℓ	$2 \cdot 0.15$	$\mathrm{kg/m^2}$
Collective lever center of mass	x_{CM}	0.300	m
Collective lever rotational stiffness	K_ℓ	15.0	N m/rad
Collective lever rotational damping	C_ℓ	3.0	N m s/rad

an underestimation of the pilot's modal mass.

The inceptor is characterized by a simple tube attached to a heavier grip. The resulting collective lever mass and inertia used for the pilot-control device models have been multiplied by 2 since all helicopters are typically characterized by dual controls mechanically connected. Collective levers are usually not balanced, with the center of mass ahead of the revolute hinge axis. Table 3 lists the pilot's biomechanical parameters obtained with and without the control inceptor dynamics when considering a reference collective lever condition of $\delta_{0_E} = 18°$ (10 % of the total excursion).

Table 3. Pilot's biomechanical data with and without the inceptor dynamics.

Characteristic	Without Inceptor Dyn.	With Inceptor Dyn.	Unit
Pilot's natural frequency	3.2	2.6	Hz
Pilot's damping ratio	30.4	34.8	%
Pilot's BDFT static gain	-3.7	-5.7	deg/g
Pilot's force gradient	10.1	10.7	N/deg

The pilot's natural frequency is reduced as a consequence of the center of mass offset. This contribution has a heavier impact when compared to the elastic term due to the balancing spring and to the collective lever equivalent inertia. The pilot's damping ratio slightly increases thanks to the viscous effect on the control device dynamics. The pilot's BDFT static gain increases in magnitude (+55 %), again due to the positive center of mass offset, while the force gradient, which is inversely linked to the pilot's NMA static gain, is subject to a small increment.

The effects of the control device dynamics on the vertical bounce stability are discussed in the next section, together with sensitivity analyses to the main parameters.

Vertical Bounce Stability Analysis

The analytical models developed in the previous sections can be exploited to perform a stability analysis of the pilot-vehicle system to vertical bounce proneness and its sensitivity to several design parameters. In this work, closed-loop stability analyses are addressed using the robust stability approach based on the usage of the Nyquist criterion for Single Input-Single Output (SISO) systems (see chapter 7 of Ref. 26). The robust approach gives both qualitative and quantitative information about the grade of stability with respect to parameters variation (Refs. 13, 27, 28).

The vertical axis loop is closed by feeding the pilot-control device BDFT to the helicopter model through the appropriate gear ratio, G_0, between the collective lever rotation and the resulting main rotor collective pitch, i.e. $\vartheta_0 = G_0 \cdot \delta_0$. In the following, a constant gear ratio has been used, considering a collective pitch range of $18°$ and the collective lever full range of $30°$, namely $G_0 = 0.6$. The collective lever input might also include an additional term δ_0' (e.g., due to a voluntary pilot model) to the pilot's BDFT, which yields

$$\delta_0 = H_{BDFT}(s)\,\ddot{z} + \delta_0'. \tag{9}$$

This rotation fed into the helicopter TF of Eq. 2 through the collective pitch gear ratio becomes

$$(1 - G_0 H_{BDFT} H_{\ddot{z}\vartheta_0})\,\ddot{z} = G_0 H_{\ddot{z}\vartheta_0}\delta_0'. \tag{10}$$

The Loop Transfer Function (LTF) is thus the coefficient of $\ddot{z}$ in Eq. 10 minus 1, namely:

$$H_{LTF} = -G_0 H_{BDFT} H_{\ddot{z}\vartheta_0}. \tag{11}$$

The contribution of the control device dynamics on the LTF can be taken into account by replacing the pilot's BDFT with the updated pilot-control device BDFT, namely $\hat{H}_{BDFT}(s)$, reported in Eq. 6a.

Robust approach

The robust stability of the SISO PVS is investigated. Robust stability indices are phase (P_m) and gain (G_m) margins. Positive margins indicate a stable system, while the stability is generally considered robust when the gain margin is at least $6\,\mathrm{dB}$ and the phase margin is at least $60°$.

In the following, the Bode diagrams of the helicopter TFs and pilot's BDFT are first compared in Fig. 4. Specifically, the transfer functions for the MH and ML helicopters between the collective pitch and the vertical acceleration show the peaks and the corresponding phase delays related to the heave and rotor coning modes. The medium-light helicopter TF is characterized by higher acceleration amplitudes when compared to the heavier rotorcraft, particularly in the frequency range of 2–4 Hz, where vertical bounce phenomena are more frequent (Ref. 3), due to the lower mass. However, the higher phase delay is associated with the heavier helicopter, hence more prone to vertical RPC events (Ref. 15). The inceptor dynamics effects on the pilot's BDFT are shown in Fig. 4(b). As expected, the collective lever dynamics increase the BDFT static gain, reducing the frequency of the pilot's biomechanical pole.

The LTF Nyquist's plots for the two helicopters are shown in Fig. 5. The worst-case scenario is obtained for the MH helicopter with the inceptor dynamics. Both the gain and phase margins are negatives (Fig. 5(a), black line), leading to an unstable system. The analysis performed on the same vehicle with an ideal lever yields a mildly unstable condition. The lighter helicopter is always stable, indicating a low sensitivity to the collective lever dynamics (Fig. 5(b)). Nonetheless, the corresponding gain and phase margins evaluated for the ML helicopter do not provide a robust condition with this lever dynamics. Table 4 summarizes the gain and phase margins obtained for the analyzed conditions. Fig. 6 shows the root locus of the MH helicopter, including the pilot's BDFT with the control inceptor dynamics. The gear ratio G_0 between the collective lever rotation and the main rotor collective pitch plays the role of the

gain on the loop transfer function. The evolution of the roots with G_0 clearly shows how the closed loop system increases the damping of the rotor coning mode at the expense of the pilot's BDFT root, shifted to the right/positive side of the Argand plane, leading to a vertical bounce phenomenon. Looking at Fig. 6 it should result clear that the presence of non-minimum phase zeros in the aircraft dynamics is at the root of the onset of this instability.

Table 4. Robust stability margins.

Pilot-Vehicle System	Gain Margin	Phase Margin
MH, w/out inceptor dyn.	$-0.66\,\mathrm{dB}$ @ $3.61\,\mathrm{Hz}$	-7.56° @ $3.71\,\mathrm{Hz}$
MH, with inceptor dyn.	$-2.04\,\mathrm{dB}$ @ $3.24\,\mathrm{Hz}$	-17.57° @ $3.52\,\mathrm{Hz}$
ML, w/out inceptor dyn.	$1.31\,\mathrm{dB}$ @ $4.51\,\mathrm{Hz}$	9.79° @ $4.28\,\mathrm{Hz}$
ML, with inceptor dyn.	$0.97\,\mathrm{dB}$ @ $4.19\,\mathrm{Hz}$	5.97° @ $4.02\,\mathrm{Hz}$

The role of the landing gear in vertical bounce proneness

The landing gear effect on vertical bounce proneness is highlighted through Figs. 7 and 8, for both the MH and ML helicopters. The heave motion in hover condition (landing gear OFF) is represented by first-order dynamics whose time constant is around $1\,\mathrm{s}$ for helicopters considered in this work. Heave dynamic, however, changes its behaviour when the helicopter is on the ground. Indeed, the viscoelastic contribution due to the landing gear leads to second-order complex and conjugate roots. The low-frequency peak is visible in the helicopter Bode diagrams (see Fig. 7(a) and Fig. 8(a)). The corresponding effect to the vertical bounce proneness is to increase the amplitude of the helicopter vertical response in the range of frequencies overlapping the pilot's BDFT, with a further reduction of the PVS stability boundaries. Consequently, on-ground conditions (take-off, landing) can be more prone to the vertical bounce phenomenon, compared to in-flight conditions.

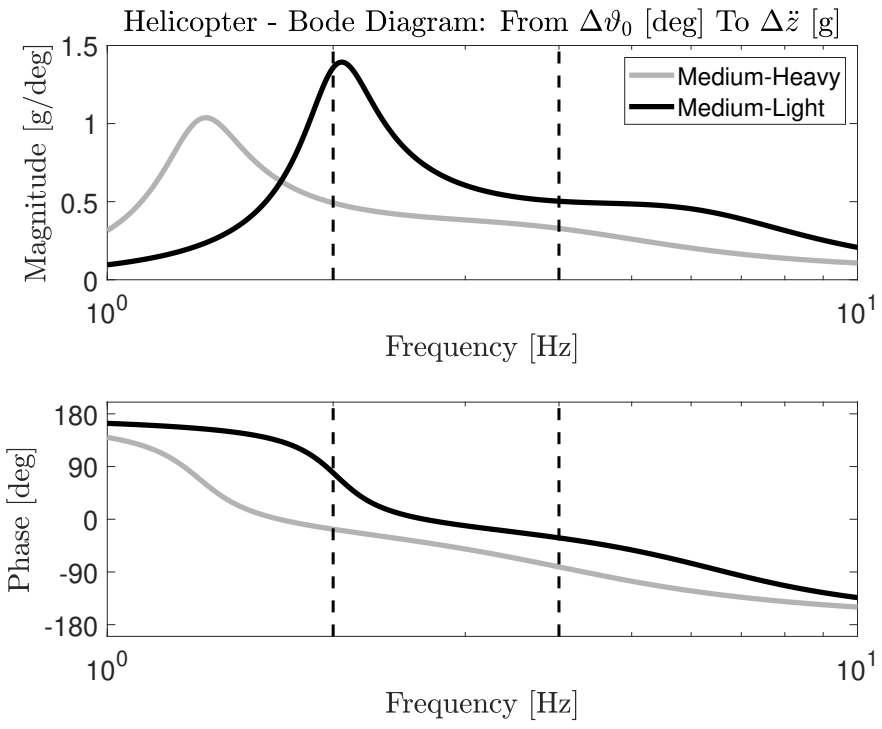

(a) Helicopter.

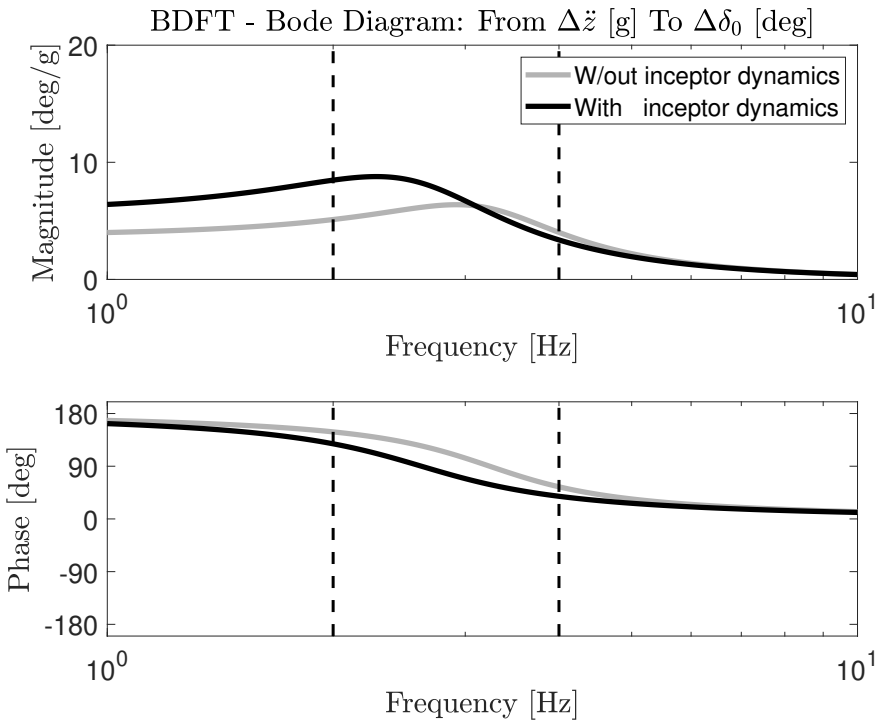

(b) Pilot's BDFT.

Fig. 4 Bode diagrams of the helicopter (top) and pilot's BDFT (bottom) transfer functions. The range of frequencies 2-4 Hz is highlighted by vertical dashed lines.

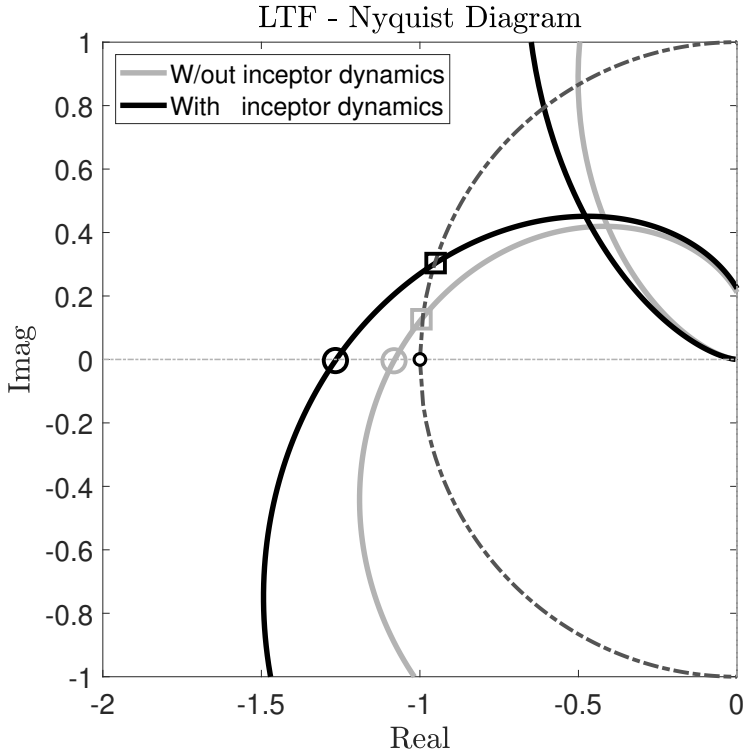

(a) Medium-Heavy.

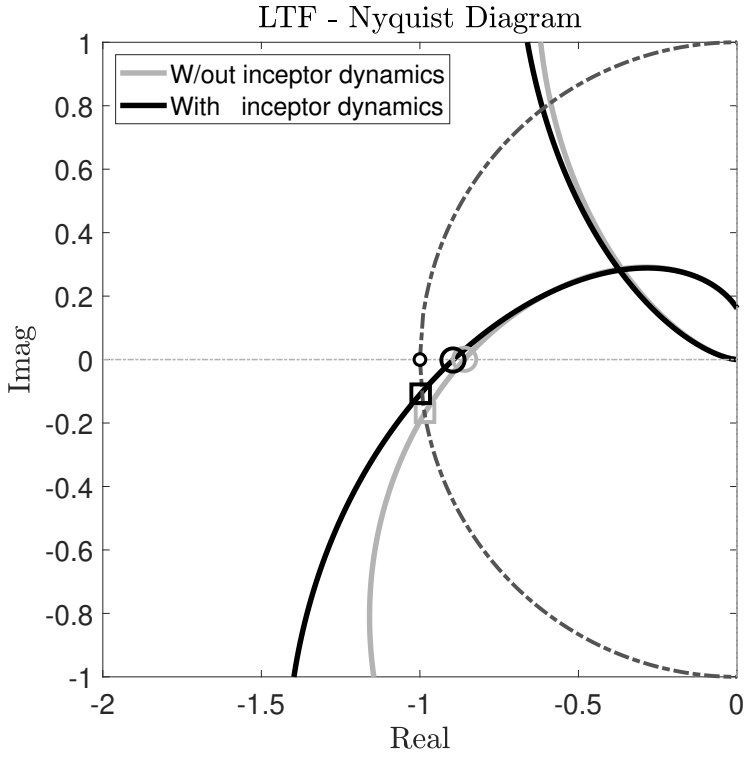

(b) Medium-Light.

Fig. 5 Nyquist diagrams of the LTF with and without the inceptor dynamics for the MH (top) and ML (bottom) helicopters. (○) gain margins and (□) phase margins points.

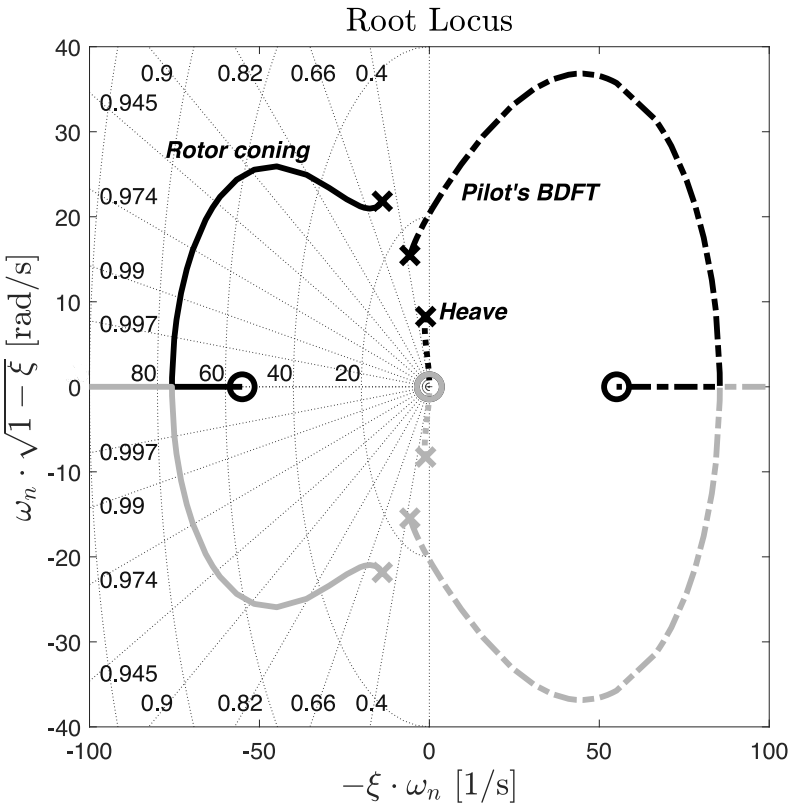

Fig. 6 Root locus of the MH helicopter with control inceptor dynamics. The poles of the system are denoted by ($\times$) while the zeros are denoted by ($\circ$).

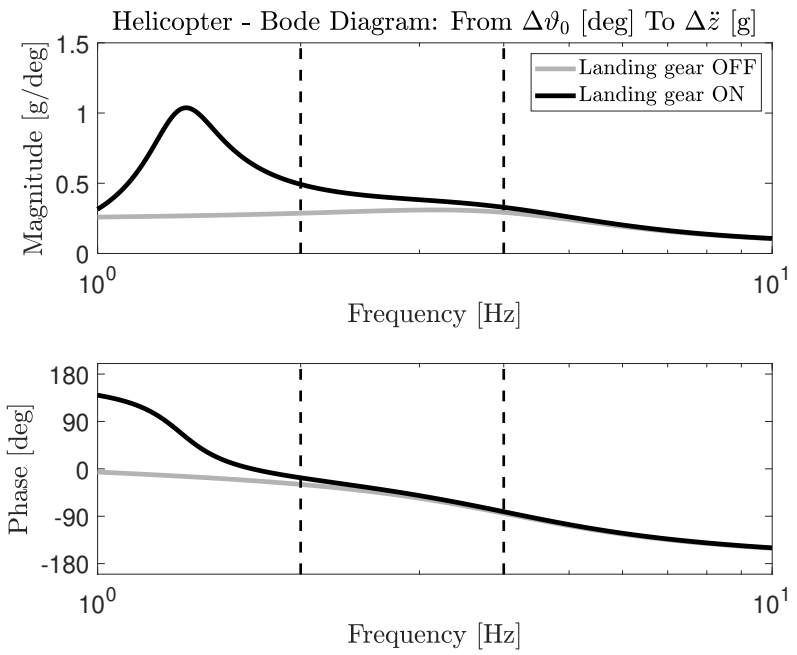

(a) Helicopter.

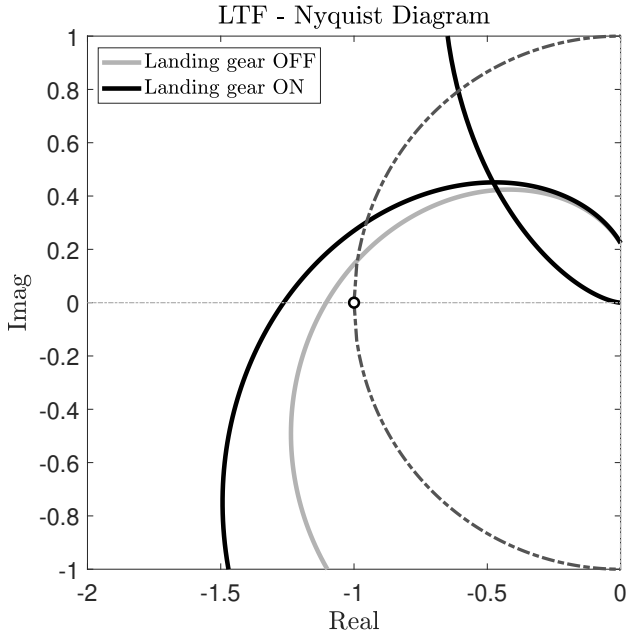

(b) Pilot-Vehicle System.

Fig. 7 Landing gear effect on vertical bounce proneness: MH helicopter.

The impact of the landing gear on the vertical bounce could be even worst if the heave mode natural frequency move closer to the rotor coning mode, as shown in Fig. 9 for the MH helicopter. Consequently,

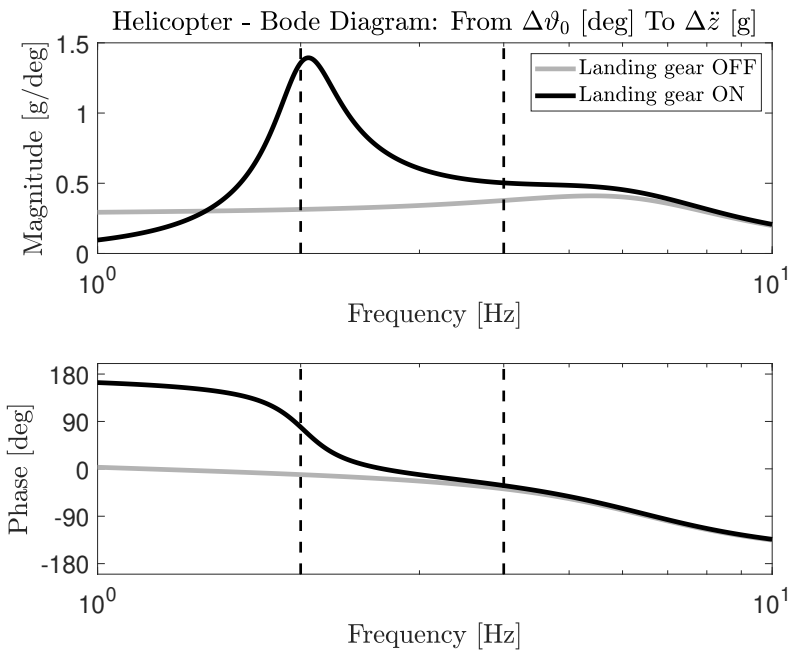

(a) Helicopter.

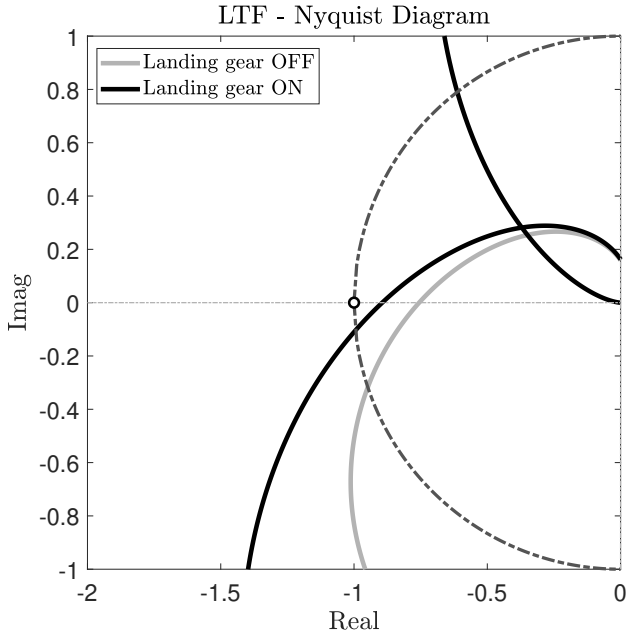

(b) Pilot-Vehicle System.

Fig. 8 Landing gear effect on vertical bounce proneness: ML helicopter.

helicopter design guidelines should recommend that the frequency of the heave mode on the ground should be sufficiently distant from the one of the rotor coning to avoid possible adverse interactions. In reality,

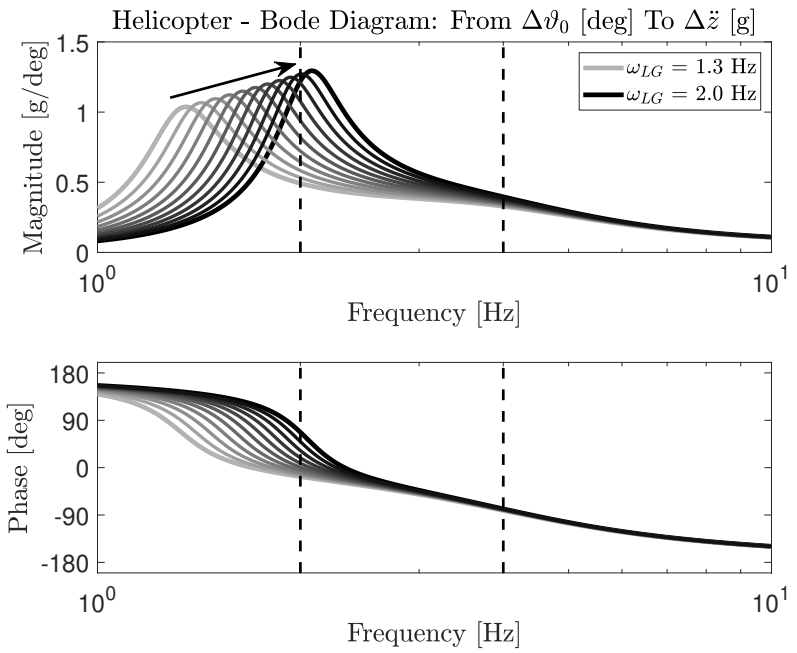

(a) Helicopter.

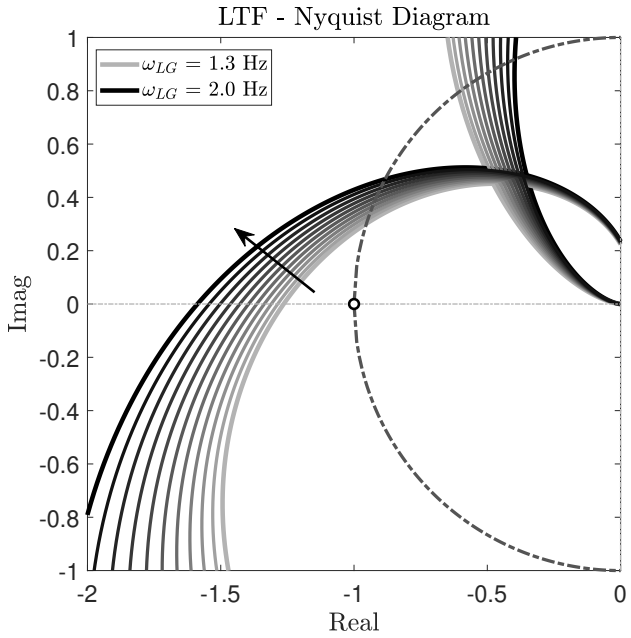

(b) Pilot-Vehicle System.

Fig. 9 Landing gear natural frequency effect on vertical bounce proneness: MH helicopter.

achieving this goal could prove to be difficult, since the coning mode frequency is constrained by the rotor aeromechanics to be close to 1/rev, and the on-ground heave mode frequency is bound by the stiffness and

the mass of the undercarriage, which are in turn constrained by numerous other design requirements. They offer, however, the greatest opportunity for intervention.

It must be remarked that the robust stability analysis results obtained with and without the landing gear have been evaluated with the same pilot's BDFT, maintaining the same reference collective lever position (i.e. $\delta_{0_E} = 10\%$). This configuration is representative of the helicopter on the ground since the main rotor collective pitch angles are small and, sometimes, negative to improve the rotorcraft's adherence to the ground. Conversely, the in-flight conditions require higher collective pitch angles and the corresponding position of the lever might range between 50% and 75% of the total excursion. Hence, robust stability analysis in hover must be evaluated with an updated pilot's BDFT, considering higher collective lever reference positions. Fig. 10 shows the evolution of the frequency and damping ratio for the PVS critical root obtained for the two helicopters, with reference to the collective lever position. The reduction of the

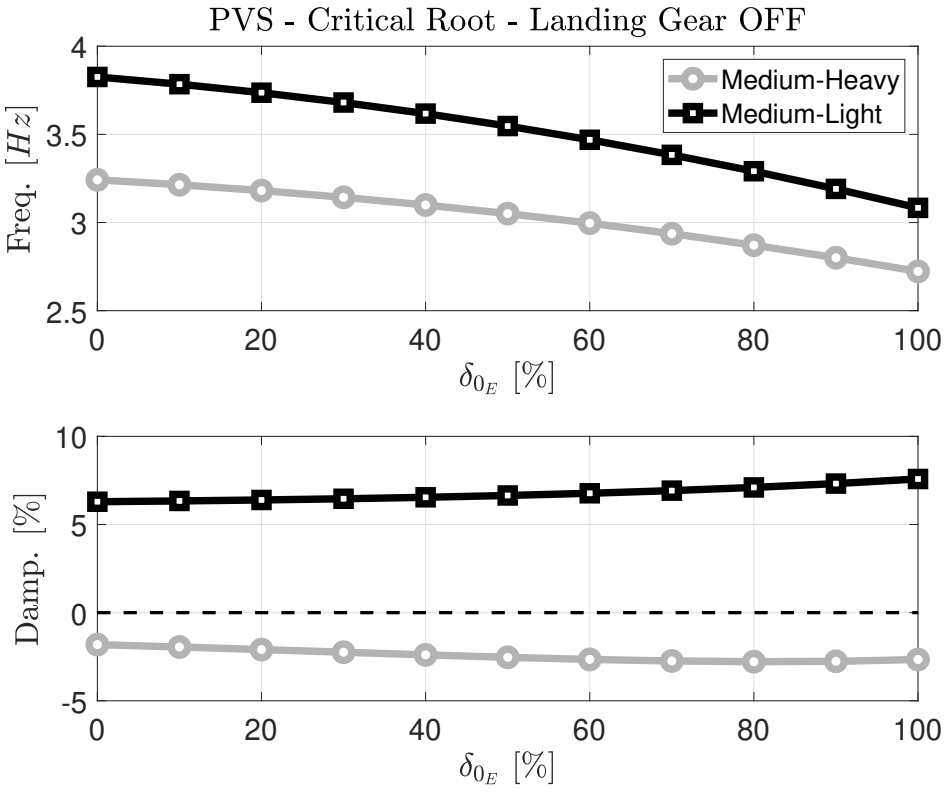

Fig. 10 Evolution of the critical root w.r.t. the collective lever reference position - PVS, Landing gear OFF.

critical root frequency is observed for both helicopters. Vertical bounce events in hover are consequently

expected at lower frequencies when compared to the same phenomena on the ground. The corresponding damping ratios show a mild sensitivity to the collective lever position, although the two helicopters exhibit different behaviours. While the damping ratio of the ML helicopter increases with higher collective lever positions, following a monotonic and stable trend, the MH helicopter is characterized by a slight reduction of the damping ratio up to collective lever reference positions of 80%, to further increase in the final stretch. Nonetheless, the heavier helicopter maintains an unstable behaviour, highlighted by the negative values of the damping ratio. This indicates that for this class of helicopters a change of loop gain may hardly achieve a stabilization of PAO.

Sensitivity of stability margins

The sensitivity of the stability index of the closed-loop pilot-vehicle system with respect to the variation of important parameters has been evaluated. The gain margin G_m has been chosen as the reference parameter for the analysis since it is guaranteed to have a finite magnitude in all possible conditions, while the phase margin magnitude grows to infinity when the LTF is completely inside the unit circle. Furthermore, the two indices yielded similar information in all the considered cases, therefore only one is shown for brevity.

The sensitivity analysis has been performed considering the variation of parameters in four categories:

- landing gear parameters: the landing gear heave mode frequency ω_{LG} and damping ratio ξ_{LG};
- operational parameters: the helicopter total mass m, the Lock number γ;
- control device parameters: the collective lever mass m_ℓ, its center of mass offset with respect to the rotation axis x_{CM};
- pilot's BDFT parameters: the pilot natural frequency ω_p and damping ratio ξ_p.

The sensitivity is visualized through two-dimensional maps, in which the color is changed according to the value of the gain margin. Three regions are identified with different color gradients:

1) the unstable region, associated with negative values of G_m, corresponding to colors ranging from red to black, the latter indicating more negative values of G_m;

2) the *simply* stable region, associated with values of the gain margin positive but less than the robust threshold, i.e. $0 \leq G_m < 6$ dB, corresponding to colors ranging from bright yellow to orange, the latter indicating smaller values;

3) the *robust* stability region, associated with values of the gain margin positive and greater than the robust threshold, i.e. $G_m \geq 6$ dB, corresponding to colors ranging from blue to green, the latter indicating larger values.

The variation of all parameters is expressed with respect to nominal reference values.

Sensitivity to landing gear parameters

Figures 11(a) and 11(b) show the gain margin G_m for the closed-loop systems composed of the Medium-Heavy (MH) and Medium-Lightweight (ML) helicopters and the pilot vertical bounce dominant mode, as a function of two critical design parameters of the landing gear: the on-ground heave mode natural frequency ω_{LG} and the associated damping factor ξ_{LG}. Trends are very similar for the two helicopters, with a decrease in the natural frequency and an increase in the damping factor proving beneficial for the coupled system stability. The reason why the latter is beneficial is straightforward, while for the first one it can be noted that a decrease in the natural frequency will lead to a greater separation between the on-ground heave mode and the other natural frequencies involved in collective bounce, namely the collective flap mode of the main rotor and the pilot biomechanical mode involving the collective lever rotation.

Sensitivity to operational parameters

Figures 12(a) and 12(b) show the LTF gain margin G_m as a function of the variation of the main rotor Lock number γ and the helicopter mass m. The Lock number is a function of air density, and thus of flight altitude, while changes in the helicopter mass are usually related to the specific helicopter configuration, often a function of the flight mission. The analysis is performed to highlight the critical design conditions for vertical bounce: it is clear from the gain margin maps that the most challenging configuration is found for the lowest helicopter mass and the highest Lock number, i.e. for low-altitude operations in low-payload

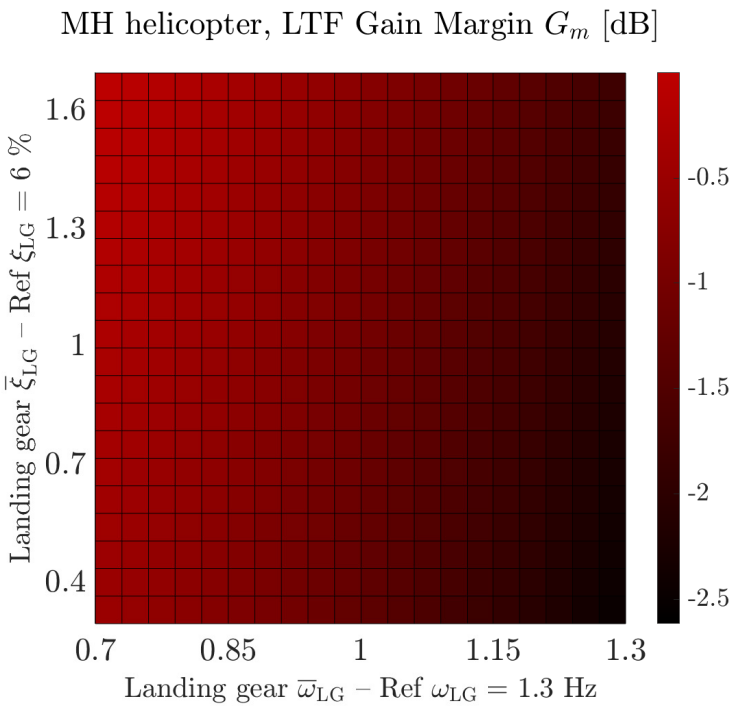

(a) MH helicopter.

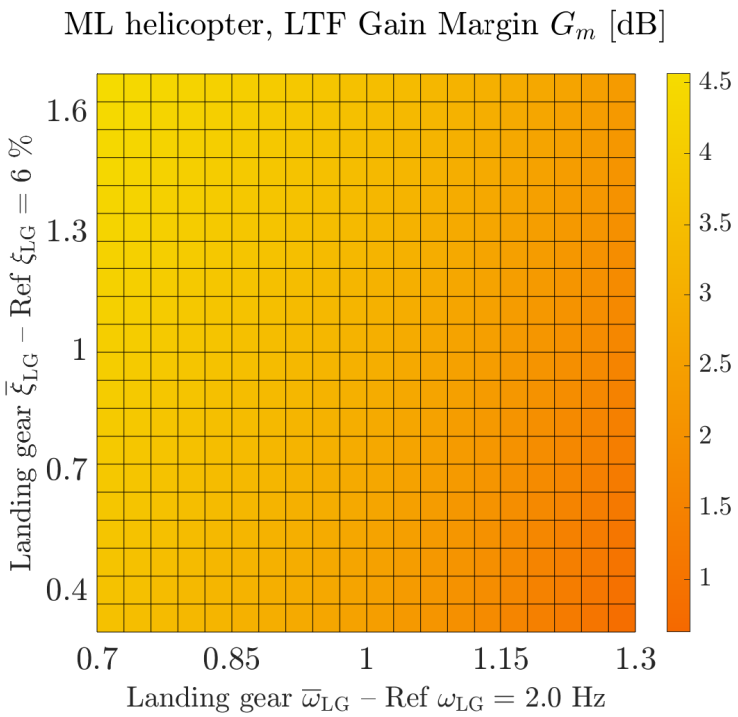

(b) ML helicopter.

Fig. 11 Sensitivity of the LTF gain margin to design parameters of the landing gear structure: ω_{LG} and ξ_{LG}.

configurations. These considerations, combined with the results found in the previous section, lead to the identification of on-ground conditions with low weight, such as the landing, as most sensitive to vertical bounce.

Sensitivity to control device parameters

The sensitivity of the vertical bounce stability margin with respect to parameters affecting the design of the control device (i.e. of the collective control chain) is shown in Figures 13, 14, and 15. The effect of the variation of the collective lever mass m_ℓ and center of mass offset x_{CM} is reported in Fig. 13, while the effect of the collective lever reference angular position δ_0 and the collective lever length ℓ is reported in Fig. 14. The first two maps show that a lightweight stick with the center of mass as close as possible to the pivot axis (i.e. as balanced as possible) is preferable to a heavier and less balanced one. The maps in Figures 14(a) and 14(b) show also that a longer collective stick is generally preferable to a shorter one, even though the trend is not always monotonic. A larger inclination of the lever with reference to the horizontal plane is also beneficial, as evidenced by the positive trend of G_m concerning the collective reference position δ_0. However, it must be highlighted that in the numerical analysis done to generate the maps shown, the change in collective lever length was not matched by a corresponding change in the static moment; the distance of the lever center of mass to the pivot axis was kept at the nominal value of $300\,\text{mm}$. While manufacturing a longer lever with the same mass as a shorter one is surely not technically impossible, changing materials and the lever design, a large variation of length not matched by a mass increment will be probably associated with a large increase in manufacturing costs and thus could become non feasible economically.

As a final remark, in Figures 15(a) and 15(b) the dependence of the stability margin with respect to a variation of the trim mechanism properties is shown, in TRIM ON conditions, i.e. with the Force Trim Release button *not* pressed. The two maps are shown to highlight that the trim mechanism can easily bring the system into robustly stable operating conditions. Furthermore, very often when the trim system is engaged, the left hand of the pilot is *not* on the collective control lever grip. Thus, the feedback path that is at the core of the vertical bounce is broken. Hence, in all the other analyses, TRIM OFF conditions

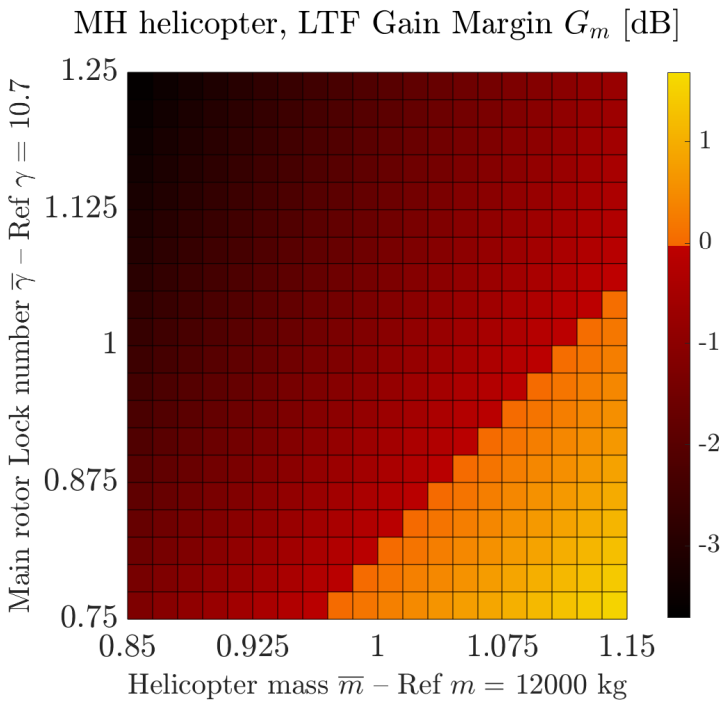

(a) MH helicopter.

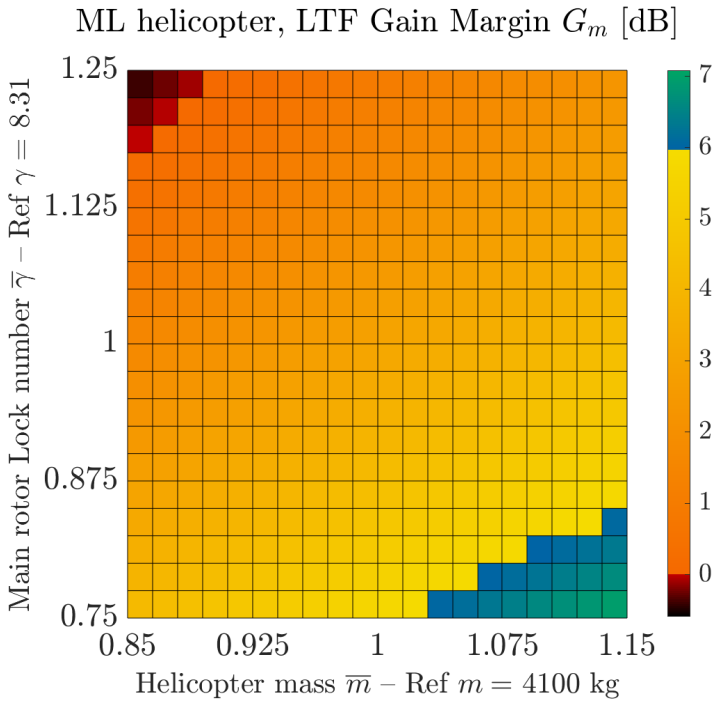

(b) ML helicopter.

Fig. 12 Sensitivity of the LTF gain margin to flight operation conditions: γ and m.

are considered, i.e. the Force Trim Release button is assumed to be pressed. The symbols K_T and C_T in Fig. 15 refer to the equivalent stiffness and damping of the trim mechanism. Notice that K_ℓ and C_ℓ refer, instead, to the stiffness and damping associated with the balancing spring and the collective friction system, which are separate mechanical components with respect to the Force Trim.

Sensitivity to pilot's BDFT parameters

The influence of the pilot's biomechanics on the LTF stability margin is shown in Figures 16 and 17. Figures 16(a) and 16(b) show the variation of G_m as a function of the natural frequency and the damping factor of the dominant biomechanical pole of the pilot for the vertical bounce. Both the frequency and the damping of the biomechanical pole are directly proportional to the closed-loop stability margin. The damping factor effect on the stability is trivial: the higher is damping the better is the gain margin. The effect on the frequency is more complex. Lower biomechanical frequencies are associated with a greater static gain of the BDFT, increasing the overall amount of energy that is transferred from the cockpit heave acceleration to the collective control inceptor rotation. They are associated with taller and heavier pilots, as already discussed in previous works (Ref. 29).

Figure 17 shows the influence of the pilot modal mass m_p, combined with the variation of the collective stick center of mass offset x_{CM} and moment of inertia to the pivot axis J_ℓ, for the MH helicopter. Increasing the modal mass, as well as increasing x_{CM}, has negative repercussions on the stability margin. The effect of J_ℓ is less pronounced and is not monotonic. The results suggest that reducing the mass of the pilot body that is free to vibrate for a collective lever movement is beneficial. Therefore, adding an armrest for the pilot's left arm, even in the form of an appropriately shaped seat backrest, which can allow the pilot to rest the upper limb portion on the side of the seat itself, can be seen as a viable solution to alleviate the vertical bounce proneness of a particular helicopter.

Conclusions

A simple yet complete analytical model has been presented to perform design parametric analysis of the vertical bounce, a particular type of pilot-assisted oscillation that can affect rotorcraft significantly. The

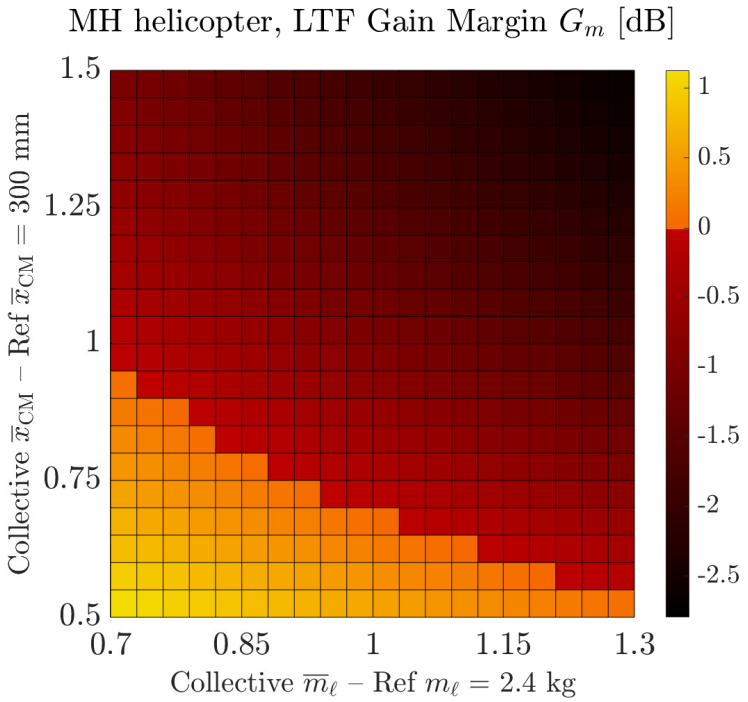

(a) MH helicopter.

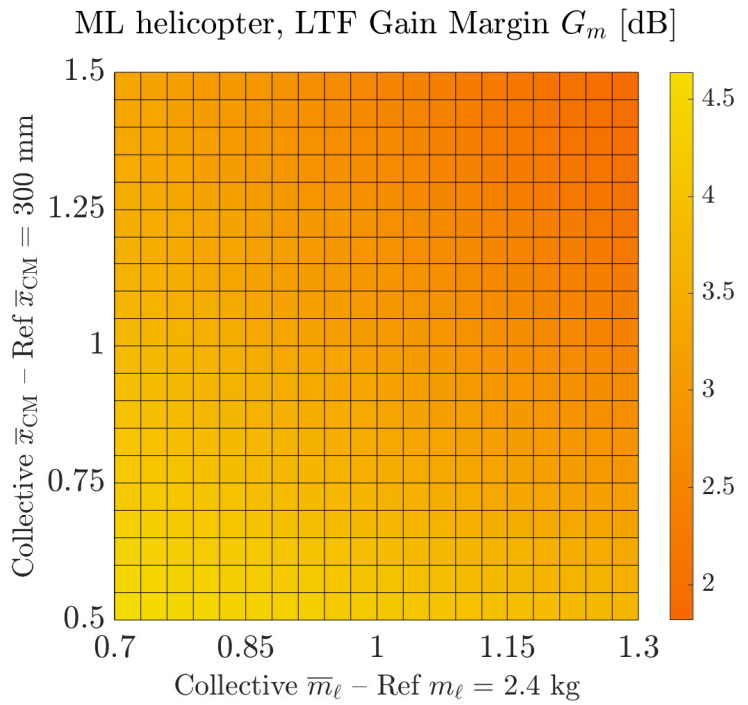

(b) ML helicopter.

Fig. 13 Sensitivity of the LTF gain margin to control device design parameters: m_ℓ and x_{CM}.

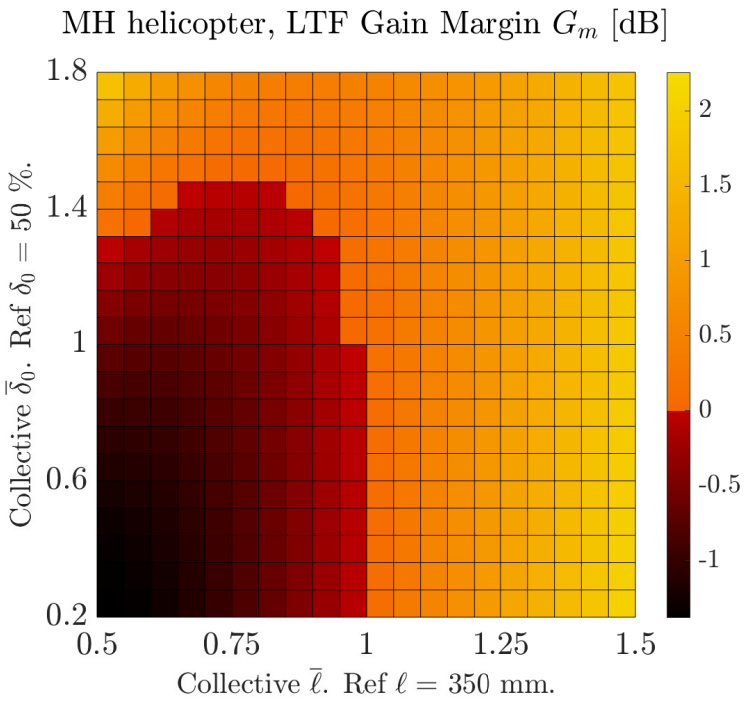

(a) MH helicopter.

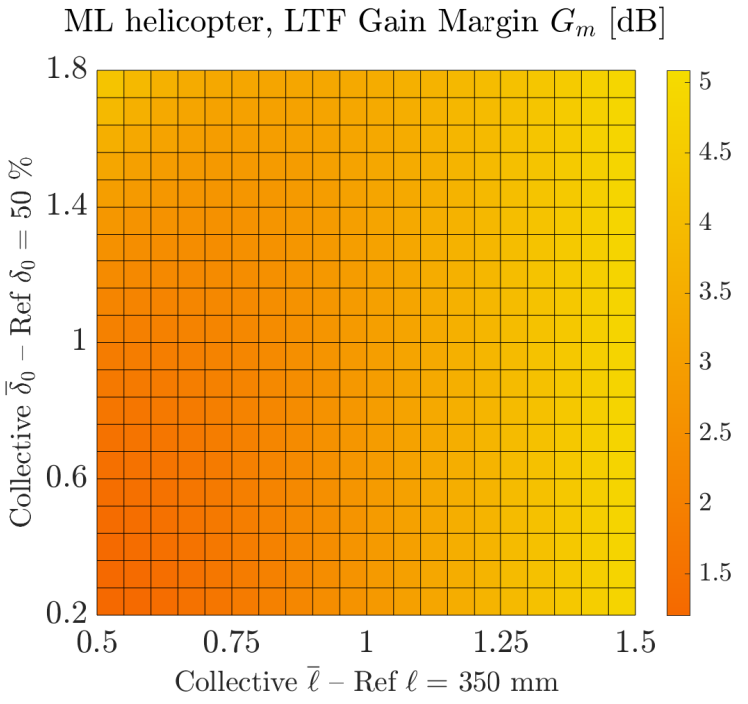

(b) ML helicopter.

Fig. 14 Sensitivity of the LTF gain margin to control device design parameters: δ_0 and ℓ.

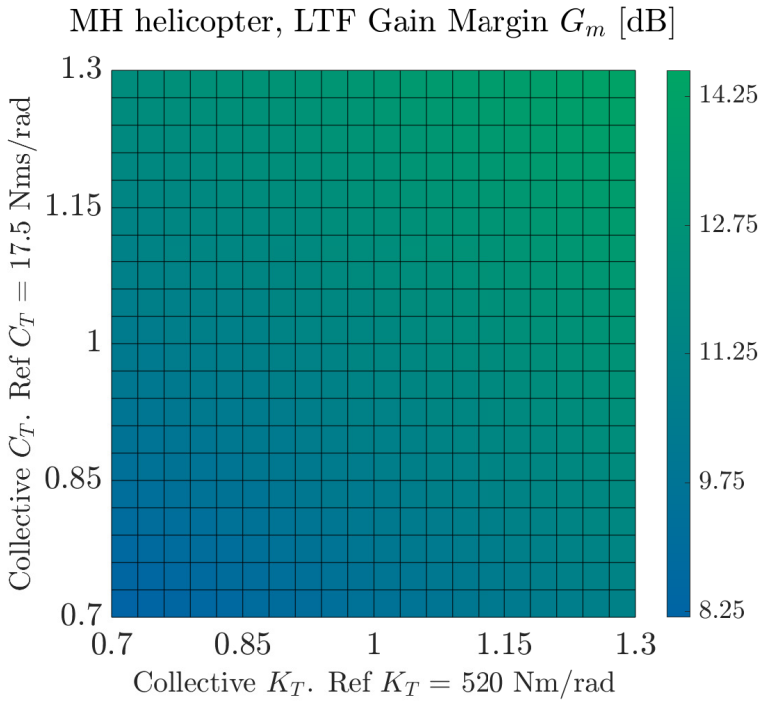

(a) MH helicopter.

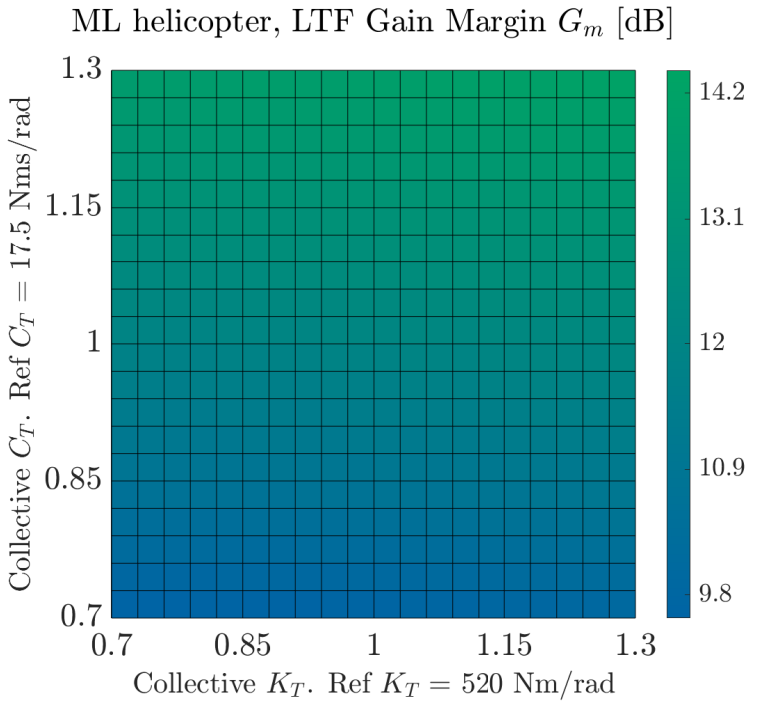

(b) ML helicopter.

Fig. 15 Sensitivity of the LTF gain margin to control device design parameters: K_T and C_T.

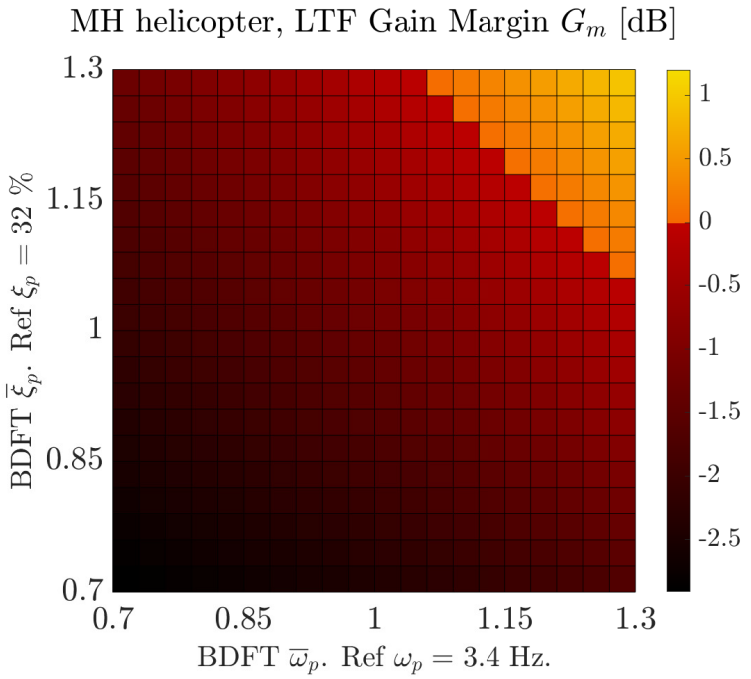

(a) MH helicopter.

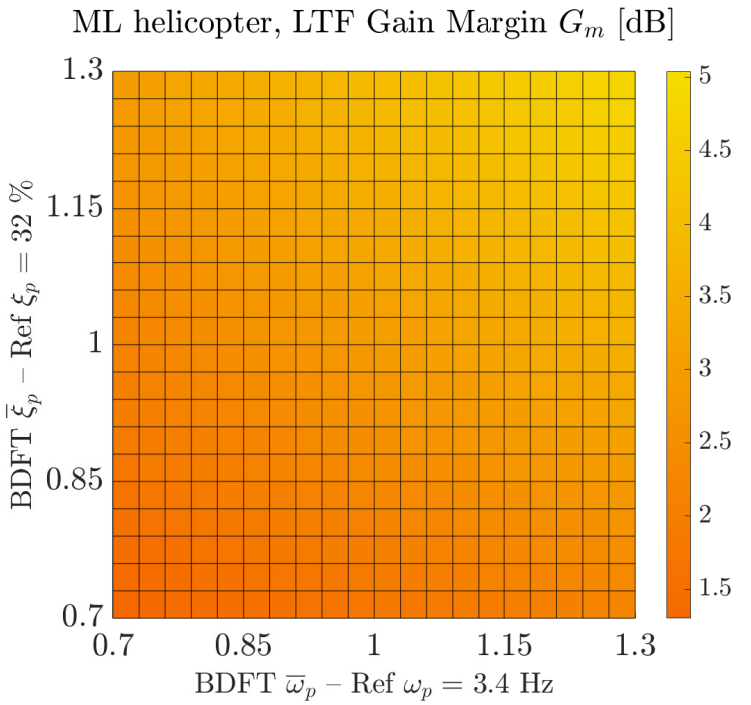

(b) ML helicopter.

Fig. 16 Sensitivity of the LTF gain margin to pilot biomechanical response parameters: ω_p and ξ_p.

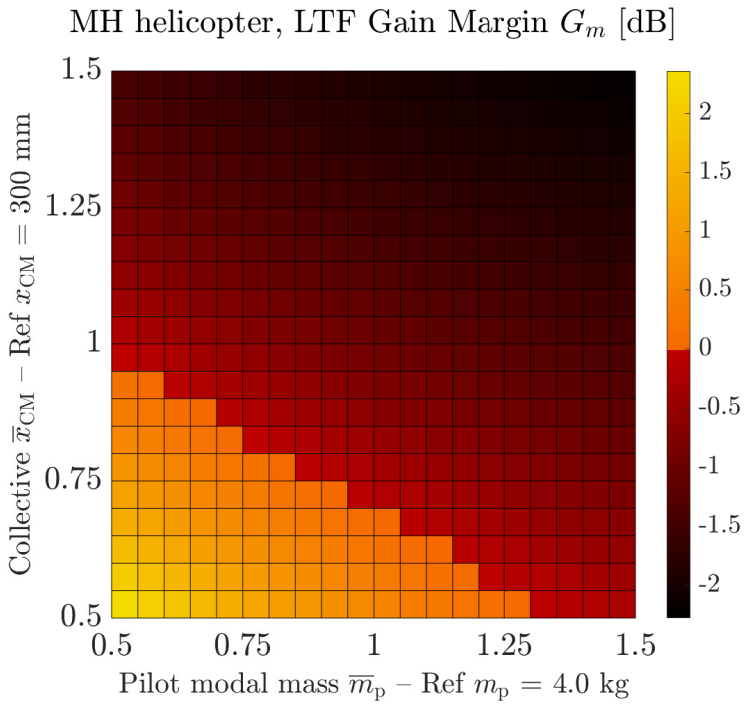

(a) Sensitivity to m_p and x_{CM}.

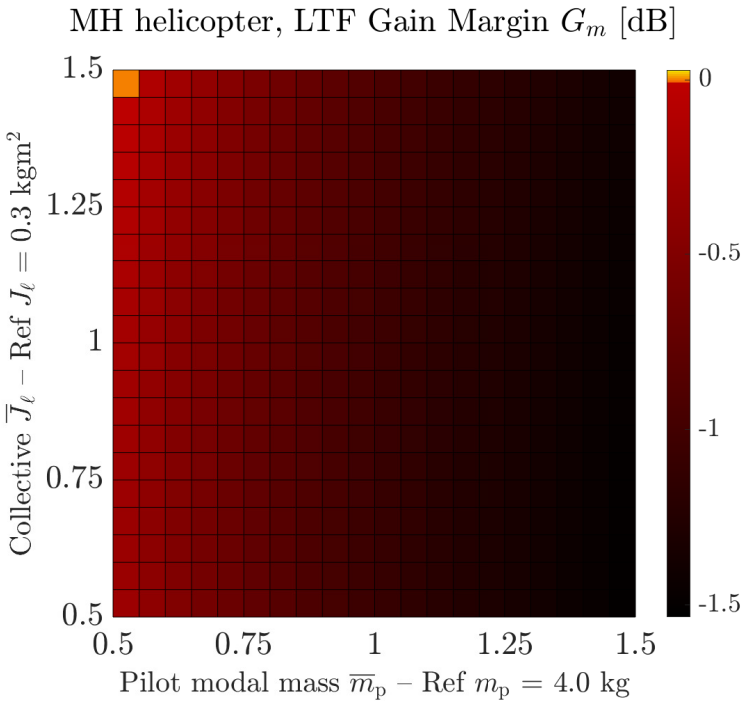

(b) Sensitivity to m_p and J_ℓ.

Fig. 17 Sensitivity of the LTF gain margin sensitivity to the variation of m_p, x_{CM} (top) and to the collective lever moment of inertia with respect to the rotation axis (bottom).

model represents a clear advancement with respect to the current state of the art since it allows to separate the contribution of pilot biodynamics and control inceptor mechanical characteristics, allowing assessing the impact of different choices for the collective lever design. The identification of on-ground conditions as the most prone to vertical bounce, shown through the sensitivity analysis, justifies the importance of modeling also the effect of landing gear that can affect significantly the heave dynamics of the helicopter when in contact with the ground.

The separation of the inceptor dynamic parameters allowed to verify that vertical bounce could be a problem only when the trim spring is disengaged. Additionally, the sensitivity to helicopter parameters showed that low altitude – low weight conditions are more subject to potential instabilities. However, this does not mean that heavy helicopters are less prone to vertical bounce, because the size brings the coning mode frequency of this class of vehicle close to the pilot's biodynamic frequency, causing a higher degree of interaction between the pilot and the aircraft dynamics. All these recommendations may be used by helicopter designers to lead to aircraft less prone to this particular type of RPC. However, sensitivity to the pilot's pole positioning and damping is significant, confirming the subjectivity of the phenomenon, considering that these parameters change among pilots but also for the same pilot depending on his physical and mental status.

Looking at the problem from the point of view of the control chain design, it has been shown that the design should focus especially on the position of the collective lever center of mass, and secondly on the length and the moment of inertia of the lever. Moving the center of mass closer to the rotation pivot, even leaving the other parameters untouched, seems a viable solution to increase the robustness to vertical bounce. Finally, an armrest device, as a means to reduce the modal mass of the pilot, can help to reduce the proneness to vertical bounce.

While more sophisticated biomechanical models can be used to unravel the relationship that exists between the voluntary and involuntary action of the pilot on inceptors, a simple model of the type presented here can help designers in taking the correct decisions to limit the potential development of RPCs that could endanger the safety of flight, particularly in the critical phases of flight close to the ground.

References

[1]Pavel, M. D., Jump, M., Dang-Vu, B., Masarati, P., Gennaretti, M., Ionita, A., Zaichik, L., Smaili, H., Quaranta, G., Yilmaz, D., Jones, M., Serafini, J., and Malecki, J., "Adverse Rotorcraft Pilot Couplings — Past, Present and Future Challenges," *Progress in Aerospace Sciences*, Vol. 62, October 2013, pp. 1–51. doi: 10.1016/j.paerosci.2013.04.003

[2]Mitchell, D. G. and Klyde, D. H., "Identifying a Pilot-Induced Oscillation Signature: New Techniques Applied to Old Problems," *Journal of Guidance, Control, and Dynamics*, Vol. 31, (1), January 2008, pp. 215–224.
doi: 10.2514/1.31470

[3]Dieterich, O., Götz, J., Dang-Vu, B., Haverdings, H., Masarati, P., Pavel, M. D., Jump, M., and Gennaretti, M., "Adverse Rotorcraft-Pilot Coupling: Recent Research Activities in Europe," Proceedings of the 34th European Rotorcraft Forum, Liverpool, UK, September 2008.

[4]Zanoni, A., Zago, M., Paolini, R., Quaranta, G., Galli, M., and Masarati, P., "On Task Dependence of Helicopter Pilot Biodynamic Feedthrough and Neuromuscular Admittance: An Experimental and Numerical Study," *IEEE, Transactions on Human-Machine Systems*, Vol. 51, (5), October 2021, pp. 1–11. doi: 10.1109/THMS.2020.3044971

[5]Walden, R. B., "A Retrospective Survey of Pilot-Structural Coupling Instabilities in Naval Rotorcraft," Proceedings of the 63rd Annual Forum of the American Helicopter Society, Virginia Beach, Virginia, May 2007.

[6]Hamel, P. G., "Rotorcraft-Pilot Coupling — A Critical Issue for Highly Augmented Helicopters?" Paper 21, AGARD-FVP Symposium on "Advances in Rotorcraft Technology", AGARD-CP-592, Gatineau, Québec, Canada, April 1997.

[7]Ockier, C. J., "Pilot Induced Oscillations in Helicopters — Three Case Studies," Technical Report IB 111-96/12, German Aerospace Center (DLR), Braunschweig, Germany, 1996.

[8]"Bell 525 Flight Test Accident," Aircraft Accident Report DCA 16FA199, Bell Helicopter Textron Inc., Italy, Texas, July 2016.

[9]Lantzsch, R., Hamers, M., and Wolfram, J., "Flight Control and Handling Qualities Evaluations

Considering Air Resonance," *Journal of the American Helicopter Society*, **59**, 022001 (2014).
doi: 10.4050/JAHS.59.022001

[10]Dryfoos, J. B., Kothmann, B. D., and Mayo, J., "An Approach to Reducing Rotor-Body Coupled Roll Oscillations on the RAH-66 Comanche Using Modified Roll Rate Feedback," Proceedings of the 55th Annual Forum of the American Helicopter Society, Montreal, Québec, Canada, May 1999.

[11]Muscarello, V., Quaranta, G., Masarati, P., Lu, L., Jones, M., and Jump, M., "Prediction and Simulator Verification of Roll/Lateral Adverse Aeroservoelastic Rotorcraft-Pilot Couplings," *Journal of Guidance, Control, and Dynamics*, Vol. 39, (1), January 2016, pp. 42–60.
doi: 10.2514/1.G001121

[12]Parham, T., Jr., Popelka, D., Miller, D. G., and Froebel, A. T., "V-22 Pilot-in-the-Loop Aeroelastic Stability Analysis," Proceedings of the 47th Annual Forum of the American Helicopter Society, Phoenix, Arizona, May 1991.

[13]Muscarello, V., Colombo, F., Quaranta, G., and Masarati, P., "Aeroelastic Rotorcraft–Pilot Couplings in Tiltrotor Aircraft," *Journal of Guidance, Control, and Dynamics*, Vol. 42, (3), March 2019, pp. 1–14.
doi: 10.2514/1.G003922

[14]Muscarello, V. and Quaranta, G., "Structural Coupling and Whirl-Flutter Stability with Pilot-in-the-Loop," *Journal of the American Helicopter Society*, **66**, 032003 (2021).
doi: 10.4050/JAHS.66.032003

[15]Muscarello, V., Quaranta, G., and Masarati, P., "The Role of Rotor Coning in Helicopter Proneness to Collective Bounce," *Aerospace Science and Technology*, Vol. 36, July 2014, pp. 103–113.
doi: 10.1016/j.ast.2014.04.006

[16]Rand, O., "Influence of Interactional Aerodynamics on Helicopter Rotor/Fuselage Coupled Response in Hover and Forward Flight," *Journal of the American Helicopter Society*, Vol. 34, (4), 1989, pp. 28–36.
doi: 10.4050/JAHS.34.28

[17]Masarati, P., Quaranta, G., and Zanoni, A., "Dependence of Helicopter Pilots' Biodynamic Feedthrough on Upper Limbs' Muscular Activation Patterns," *Proceedings of the Institution of Mechanical Engineers, Part K: Journal of Multi-body Dynamics*, Vol. 227, (4), December 2013, pp. 344–362.
doi: 10.1177/1464419313490680

[18]Zanoni, A., Cocco, A., and Masarati, P., "Multibody Dynamics Analysis of the Human Upper Body for Rotorcraft–Pilot Interaction," *Nonlinear Dynamics*, Vol. 102, (3), October 2020, pp. 1517–1539.
doi: 10.1007/s11071-020-06005-7

[19]Allen, R. W., Jex, H. R., and Magdaleno, R. E., "Manual Control Performance and Dynamic Response During Sinusoidal Vibration," Technical Report 73–78, Aerospace Medical Research Laboratory, Wright–Patterson Air Force Base, OH, October 1973.

[20]Jex, H. R. and Magdaleno, R. E., "Biomechanical Models for Vibration Feedthrough to Hands and Head for a Semisupine Pilot," *Aviation, Space, and Environmental Medicine*, Vol. 49, (1–II), January 1978, pp. 304–316.

[21]Höhne, G., "Computer Aided Development of Biomechanical Pilot Models," *Aerospace Science and Technology*, Vol. 4, (1), January 2000, pp. 57–69.
doi: 10.1016/S1270-9638(00)00117-6

[22]Mayo, J. R., "The Involuntary Participation of a Human Pilot in a Helicopter Collective Control Loop," Paper 81, Proceedings of the 15th European Rotorcraft Forum, Amsterdam, Netherlands, September 1989.

[23]Masarati, P., Quaranta, G., and Jump, M., "Experimental and Numerical Helicopter Pilot Characterization for Aeroelastic Rotorcraft-Pilot Couplings Analysis," *Proceedings of the Institution of Mechanical Engineers, Part G: Journal of Aerospace Engineering*, Vol. 227, (1), January 2013, pp. 124–140.
doi: 10.1177/0954410011427662

[24]Venrooij, J., Abbink, D. A., Mulder, M., van Paassen, M. M., and Mulder, M., "Biodynamic Feedthrough is Task Dependent," Proceedings of the 2010 IEEE International Conference on Systems Man and Cybernetics (SMC), Istanbul, Turkey, October 2010.
doi: 10.1109/ICSMC.2010.5641915

[25]Zanlucchi, S., Masarati, P., and Quaranta, G., "A Pilot-Control Device Model for Helicopter Sensitivity to Collective Bounce," Paper DETC2014-34479, Proceedings of the ASME 2014 International Design Engineering Technical Conferences and Computers and Information in Engineering Conference (IDETC/CIE), Buffalo, New York, August 2014.
doi: 10.1115/DETC2014-34479

[26]Skogestad, S. and Postlethwaite, I., *Multivariable Feedback Control*, John Wiley & Sons, Chichester, UK, 2005, Chapter 7.

[27]Quaranta, G., Muscarello, V., and Masarati, P., "Lead-Lag Damper Robustness Analysis for Helicopter Ground Resonance," *Journal of Guidance, Control, and Dynamics*, Vol. 36, (4), July 2013, pp. 1150–1161.
doi: 10.2514/1.57188

[28]Muscarello, V., Masarati, P., and Quaranta, G., "Robust Stability Analysis of Adverse Aeroelastic Roll/Lateral Rotorcraft-Pilot Couplings," *Journal of the American Helicopter Society*, **62**, 022003 (2017).
doi: 10.4050/JAHS.62.022003

[29]Zanoni, A. and Muscarello, V., "Moving Towards A-Priori Identification of Undesirable Pilot Biometrics for Collective Bounce Instability," Proceedings of the 43rd European Rotorcraft Forum, Milano, Italy, September 2017.